Published by
NIGERIAN SOCIETY OF PHYSICAL SCIENCES
Available online @ https://journal.nsps.org.ng/index.php/jnsps

J. Nig. Soc. Phys. Sci. 4 (2022) 588

Journal of the Nigerian Society of Physical Sciences

Statistical Analysis and Distribution of Global Solar Radiation and Temperature Over Southern Nigeria

M. A. Okono[a], E. P. Agbo[b,*], B. J. Ekah[a], U. J. Ekah[b], E. B. Ettah[b], C. O. Edet[b,c,d]

[a]*Department of Physics, University of Calabar, Nigeria*
[b]*Cross River University of Technology, Calabar, Cross River State, Nigeria*
[c]*Faculty of Applied and Human Sciences, Universiti Malaysia, Perlis, Malaysia*
[d]*Faculty of Electronic Engineering Technology, Universiti Malaysia, Perlis, Malaysia*

Abstract

The intensity of solar energy that is received by a particular location is affected by most meteorological conditions including, the solar irradiance received by the location, precipitation, extreme heat as a result of the surface or ambient temperature, etc. We obtain the monthly global solar irradiation and ambient temperature for the three (3) eco-climatic zones in the south of Nigeria (17 locations) for 12 years (2005 - 2016) from the Photovoltaic Geographical Information System (PVGIS) Satellite. The goal of this study is to understand how regional meteorological conditions affect radiation and temperature reception. Monthly and annual trends were plotted and compared for both variables in each region to show the similarity or dichotomy in their trends. The Mann-Kendall (M-K) trend test has been adopted to reveal the changes in the variations on an annual basis, and results showed that the trend were not significant for both variables. Box plots have been used to give a better description of the data, and compared to show similarities and differences. Finally, we adopted the Gaussian (normal) distribution to show, understand and compare the data distribution. Linear regression plots for each zone shows that the relationship between the solar irradiation and temperature is high. Results show that the climate and vegetation of a region contributes majorly to the variation of radiation and temperature. Inhomogeneity of data or results for locations in the same zones may be attributed to local meteorological conditions. The results obtained here will prove vital in decision making relating to the adoption of solar energy technologies in the region. Results show that the climate and vegetation of a region contributes majorly to the variation of radiation and temperature. Inhomogeneity of data or results for locations in the same zones may be attributed to local meteorological conditions.

DOI:10.46481/jnsps.2022.588

Keywords: Global solar radiation, temperature, box plots, Mann-Kendall test, Sen's slope estimate, Gaussian distribution, linear regression

Article History:
Received: 15 January 2022
Received in revised form: 24 June 2022
Accepted for publication: 12 July 2022
Published: 14 August 2022

Communicated by: S. J. Adebiyi

1. Introduction

Careful study of the world's economy shows the importance of solar energy (directly related to global solar radiation and temperature) to economic growth [1, 2]. Many developing countries in Africa have this flaw of not being able to develop systems to put them in the position of producing enough less expensive energy despite the potential of Africa as a continent [3]. This inefficiency in solar energy conversion causes the poverty and under development activities for low GDP countries [4].

*Corresponding author tel. no: +234(0)7018774580
Email address: emmanuelpaulagbo@gmail.com (E. P. Agbo)

Usage of fossil fuels and wood for example, causes harm on a long term to these regions [5, 6]. This shows that global solar radiation is one of the environmentally friendly source of energy for the climate system and has an amount that varies with respect to the geographical location, altitude, atmospheric conditions, among others [4].

This study seeks to unravel the ambiguity of the variation of these most important variables in solar energy. These are arguably the climatic variables with the most effect on a region's solar energy variation [7–11]. A good understanding of climate change and projected trends of these two variables is very important for policymakers and/or industry managers to undertake project planning and/or installing solar cells in a considered locality. Many studies across the world have been carried out for highlighting the changes, trends and variability analysis of the solar irradiance and temperature. [12-18], but the problem is that little or no study has focused on the regional variations of a country, this study in particular is unique in that it focuses on all major cities (stations) in a country like Nigeria. The assumption is that locations in the same region have the same variation, but this may not be entirely so as latitudes, elevation, and other local meteorological factors vary.

Abdulkarim *et al.* [19] analysed solar radiation and climate data's effects generally (including on economics) on the development of solar photovoltaic (PV) systems in Nigeria. With one location for each radiation region, results showed that the southern station of Port Harcourt had the lowest viability for solar energy conversion when compared to Maiduguri and Minna. Their results also showed a positive relationship between solar radiation and temperature for all stations, while showing a negative linear relationship between solar radiation and relative humidity. The horizontal surface solar radiation (or Global Horizontal Radiation) and temperature levels for stations in southern Nigeria were evaluated using NASA SSE data by Dike *et al.* [20]. Results summarized that there is a potential for more adoption of solar energy in the region in spite of recorded lower levels. Ohunakin *et al.* [21] developed six (6) empirical models (linear and quadratic) based on ambient temperature and sunshine parameters for the southern region of Osogbo. Results showed that the temperature based models had the lowest statistical error, and therefore showed the best agreement with measured data, making it suitable for the estimation of global solar radiation. They went further to conclude that this is so for locations with the same latitude. This clearly proves the connection between the two parameters. Another study which applied solar radiation models was that of Okundamiya *et al.* [22]. Using twenty-two (22) years data for Abuja, Sokoto and the southern station of Benin City, confirmed results by Ohunakin *et al.* [21] after applying the multivariate regression relationship deduced after estimations has been made that air temperature ratio, maximum air temperature, among others performed better than other relationships.

This study however is focused on analyzing the global solar radiation and temperature variations in 17 locations of the southern eco-climatic zones of Nigeria (The guinea savannah, the tropical rainforest and the mangrove swamp. Monthly trends for radiation and temperature for all locations (17) in each zone of the southern region will plotted and compared with each other, the same will be done for the annual trends. The Mann-Kendall (M-K) trend test has been applied to discern the significance of the increasing or decreasing radiation and temperature trends. Two-dimensional Gaussian distributions as well as box plots were used to show the nature of the distribution. Results can be applied to aid in the knowledge of these variables in the region to better understand its climate dynamics like understanding the potential of global solar radiation reception for renewables and vegetation.

2. Methodology

Various methods have been utilized to analyse the data obtained. These methods include the use of box plots to describe data and linear regression (LR) plots between radiation and temperature to give a better understanding of the relationship between the variations of both. Kernel density Estimation (KDE) plots have also been used to better explain the distribution of data.

2.1. Theoretical Review

Box plots shows a graphical summarization of data. Unlike the KDE, it does not give a detailed representation of the data distribution, but gives an indication of the skewness of data. Box plots summarizes data in the following way;

Lower extreme/minimum ($Q1 - 1.5 \times IQR$), Lower quartile (Q1), median (Q2), upper quartile (Q3) and upper extreme ($Q4 = Q3 + 1.5 \times IQR$).

We use the (KDE) to examine the features and distributions of observations. The KDE takes into account the probability density function (PDF) for a normal distribution.
For a univariate KDE, the PDF is given as [23].

$$f(x|\mu,\ \sigma^2) = \frac{1}{\sqrt{2\pi\sigma^2}} exp\left[-\frac{1}{2\sigma^2}(x-\mu)^2\right] \tag{1}$$

where, σ is the standard deviation and μ is the mean.

From Equation (1), the 'argument' exponential function $\frac{1}{2\sigma^2}(x-\mu)^2$ is a quadratic function of x. This can be seen as a parabola which points downward (as evident from Gaussian/normal distributions); this is because the quadratic function has a negative coefficient [24].

The term in front of the exponential function $\frac{1}{\sqrt{2\pi\sigma^2}}$ from equation (1) is the coefficient of the function (a constant) which does not depend on x. In simple terms, this is a normalization factor that warrants that;

$$\frac{1}{\sqrt{2\pi\sigma^2}} \int_{-\infty}^{\infty} exp\left[-\frac{1}{2\sigma^2}(x-\mu)^2\right] = 1. \tag{2}$$

We can simplify Equation (1) by assuming a standard deviation (σ) of 1 and a mean (μ) of 0.

$$f(x) = \frac{1}{\sqrt{2\pi}} exp\left(-\frac{x^2}{2}\right). \tag{3}$$

The Equation (3) is a simplification of the one-dimensional (1D) Gaussian kernel function which has been employed in this study.

The Linear regression function is used to show the relationship between two variables (dependent and independent). In the case of a simple linear regression we have one independent and one dependent variable [23]. It is given by

$$Y = \pm mX \pm c + e, \tag{4}$$

where Y is the dependent variable, X is the independent variable, m is the value of the slope, c is the intercept and e is the residual error.

2.2. Test for Trend (The Mann-Kendall Trend Test)

We use the M-K test when analysing time-series data. The test is non-parametric and does not require the data to conform to a particular distribution. [10, 25-26]. We apply this test when a given range of data x_j agrees with the relation;

$$x_j = f(t_i) + \epsilon_i, \tag{5}$$

$f(t_i)$ here is a function of continuously increasing or decreasing monotonically, ϵ_i are the range residuals.

In the M-K test, we test the null hypothesis H_o which says that there is no trend, and the alternative hypothesis H_1 which means that there is a trend in the series. If the results gotten from the test agrees with the null hypothesis (meaning that there is no trend), it means that the given data x_i is randomly ordered in time (t), while the alternative hypothesis says that there is either an increasing monotonic or a decreasing monotonic trend [27-29].

The M-K test uses the statistic S, calculated using;

$$S = \sum_{k=1}^{n-1} \sum_{j=\lambda=1}^{n} sgn(x_j - x_k), \tag{6}$$

where;

$$sgn(x_j - x_k) = \begin{cases} +1; & \text{if}(x_j - x_k) > 0 \\ 0; & \text{if}(x_j - x_k) = 0 \\ -1; & \text{if}(x_j - x_k) < 0 \end{cases} \tag{7}$$

The number of data values is represented by n. A positive S value indicates an upward variation, and a negative S value characterizes a downward variation.

The normal approximation (Z statistic) is always used if the number of data values n is from 10 and above. We should also note that when there are tied/equal values, the accuracy of using the Z statistic will reduce if the data values are close to 10.

To compute the value of the Z statistic, the variance of $S'VAR(S)'$ is used [25]

$$VAR(S) = \frac{1}{18}\left[n(n-1)(2n+5) - \sum_{p=1}^{g} t_p(t_p-1)(2t_p+5)\right] \tag{8}$$

g represents the number of tied groups in the series (showing that the test takes the tied or equal values into consideration. The number of data values in the p^{th} group is represented by t_p.

The test statistic Z is now obtained using the values of $VAR(S)$ and S [25];

$$Z = \begin{cases} \frac{S-1}{\sqrt{VAR(S)}}; & S > 0 \\ 0; & S = 0 \\ \frac{S+1}{\sqrt{VAR(S)}}; & S < 0 \end{cases} \tag{9}$$

The decreasing variation is discerned from a negative Kendall Z value, and an increasing trend is seen from a positive Z value. Both interpretations can be concluded to have a significant trend if and when the data's p-value is lower than the significance level ($< 5\% = 0.05$ in this case). The trend is not significant if the p-value is higher than the level of significance [30].

3. Study Location

Nigeria is lies between longitude 2 ^oE and 15 ^oE and latitude 4 ^oN and 14^oN, having two major seasons, wet and dry [31]. The country is situated just above the geographical equator and this results to high sunshine intensity. This study is focused on the analysis of temperature and global solar radiation for the southern eco-climatic region, and figure 1a shows all states in the southern region and 1b shows the eco-climatic region as well as the locations in study. The region is characterized by her proximity to the Atlantic Ocean [32]. Table 1 gives more information about each location.

3.1. Data Source and Method of Analysis

Monthly data for average ambient temperature in Celsius and the total monthly GSR (Global Global solar radiation) in $kWh/m^2/mo$ were obtained from the PVGIS (photovoltaic geographical information system) for twelve years (2005-2016) at https://re.jrc.ec.europa.eu/pvg_tools/en?tools.html#PVP.

The total monthly GHI ($kWh/m^2/month$) for all southern locations converted to average daily GHI in mega joules ($MJ/m^2/day$) and further analyzed with the average daily temperature (in Celsius).

The analysis tool for this study is the Microsoft Excel software, which was used for the data conversion, storage and wrangling. Data visualization was carried out by the Python programming language. All graphical representations and some statistical analysis were implemented. Packages in python programming like sklearn, seaborn, matplotlib, pandas, and numpy etc., were utilized for representations including box plots, linear regression, 1D KDE plots. All were compared for all locations in each zone.

The 2D KDE employed the two (2) random variables (radiation and temperature) for its implementation. Temperature represented the x-axis and radiation represented the y-axis.

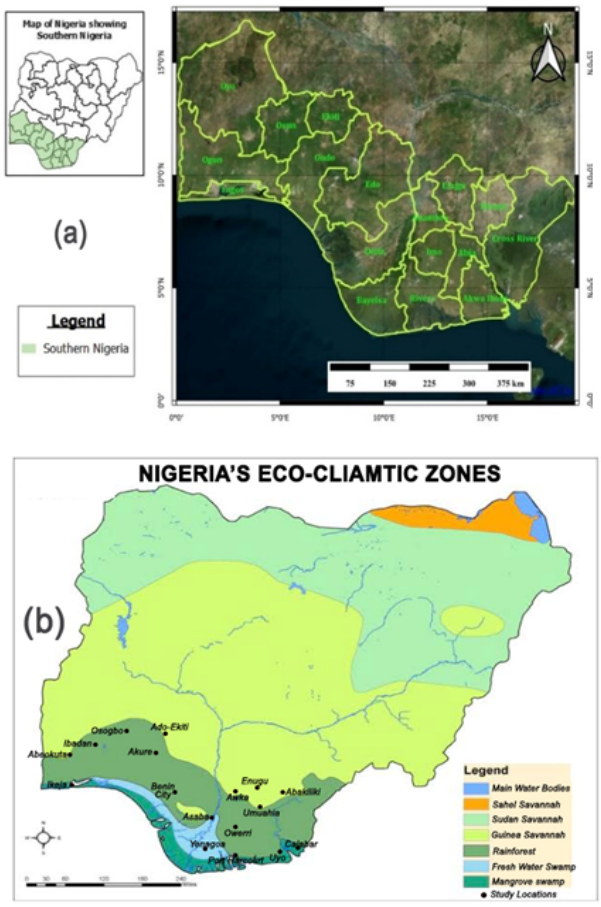

Figure 1. : (a) Map of Nigeria showing the southern region (b) Map of Nigeria showing the distribution of al eco-climatic zones, with the exact locations of the stations being studied.

Table 1. Elevation and Location (coordinates) of all study locations.

Location(State)	Elevation (m)	Latitude (^oN)	Longitude (^oE)
Abeokuta (Ogun)	30	7.155	3.339
Ado-Ekiti (Ekiti)	375	7.601	5.273
Akure (Ondo)	354	7.258	5.218
Ibadan (Oyo)	217	7.371	3.964
Ikeja (Lagos)	41	6.626	3.361
Osogbo (Osun)	352	7.754	4.581
Asaba (Delta)	44	6.025	6.693
Calabar (Cross River)	13	4.977	8.313
Benin City (Edo)	88	6.325	5.607
Port Harcourt (Rivers)	10	4.814	7.080
Uyo (Akwa Ibom)	73	5.048	7.907
Yenagoa (Bayelsa)	16	4.904	6.234
Abakiliki (Ebonyi)	46	6.312	8.107
Awka (Anambra)	103	6.218	7.083
Enugu (Enugu)	199	6.463	7.542
Owerri (Imo)	73	5.490	7.034
Umuahia (Abia)	154	5.525	7.517

4. Results and Discussion

4.1. Monthly trends

Figures 2a, 2b, and 2c show the monthly variation of radiation for the Guinea savannah, mangrove swamp and tropical rain forest regions respectively. They all have their lowest values between the months of July and August (July mostly). This variation corresponds approximately with the month (s) that have the lowest recorded temperature (Figures 2d, 2e, and 2f) in the study areas. The radiation trend steadily reduces from January till it reaches its minimum value in July, and then rises steadily between September and December.

These radiation trends (Figures 2a, 2b, and 2c) correlates positively with that of the ambient temperature (Figures 2d, 2e, and 2f). The significant difference between the monthly trends of radiation and temperature for all locations is that while the peak radiation value for the locations are observed to be in January (on average), the peak ambient temperatures are observed to be in the month of March (on average). This may be attributed to the inclusion or the increased longwave radiation around the months of March with in agreement with Soneye *et al.* [33]. The sky is clear and have no clouds from December through February, but the clouds begin to form in the month is March when rainfall begins. This increases the diffused radiation as the clouds acts as a greenhouse gas [34].

Figures 3 and 4 shows the mean radiation and temperature trends respectively for the 3 zones in study. They show that the mangrove swamp zone has lower values of temperature in the dry months (January - April), and relative to other zones, her temperature value is higher in the wet months. This could be attributed to the fact that the mangrove swamp zone has a closer proximity to the Ocean than other regions in the south. Figures 2b and 2e proves this as it shows that Calabar, Asaba, Yenegoa, and Uyo all have low values due to their close proximity to the Atlantic Ocean.

The hottest locations from the monthly trends include Abakiliki and Lagos, having monthly temperature trends that are far above others; this can be attributed to the industrial activities in those locations [35]. From Figure 4, we can see that the months with the lowest temperature values corresponds to months in the rainy/wet season which runs between the months of June and October approximately.

4.2. Annual Trends

Results were gotten for the annual global solar radiation variations for the Guinea savannah, mangrove swamp and tropical rain forest regions in Figures 5a, 5b and 5c; and for the ambient temperature variations for the Guinea savannah, mangrove swamp and tropical rain forest regions in Figures 5d, 5e and 5f respectively. Sen's slope is represented for all the aforementioned Figures in Table 2 and Table 3.

From just mere observation, we can see from the figures that the annual radiation trends steeply increased in the latter parts of the trend. The trends for the average ambient temperature are relatively stable across all years.

Figures 6 and 7 show the radiation and ambient temperature trends respectively for all southern zones. From Figure 6, we can see that the radiation variation representation for the mangrove swamp zone is the lowest among all zones. If we compare this variation to that of ambient temperature in Figure 7, we will observe that all temperature trends for all zones are

Table 2. The M-K trend test results for global solar radiation showing the nature of each of their across all years (2005 - 2016).

Location	Kendall's Tau	Mann Kendall's Statistic (S)	Test Statistic (S)	p-value (Two-tailed)	Intercept	Sen's slope (Q)	Test Interpretation	trend
Abakiliki	-0.212	-14	-0.89	0.37	19.38	-0.008	FALSE	NST (↓)
Awka	-0.212	-14	-0.89	0.37	18.95	-0.026	FALSE	NST (↓)
Enugu	-0.273	-18	-1.17	0.24	19.24	-0.025	FALSE	NST (↓)
AdoEkiti	-0.061	-4	-0.21	0.84	19.54	-0.005	FALSE	NST (↓)
Umuahia	-0.273	-18	-1.17	0.24	18.49	-0.030	FALSE	NST (↓)
Owerri	-0.212	-14	-0.89	0.37	18.44	-0.024	FALSE	NST (↓)
Port Harcourt	-0.030	-2	-0.07	0.95	16.68	-0.009	FALSE	NST (↓)
Osogbo	0.061	4	0.21	0.84	18.92	0.019	FALSE	NST (↑)
Benin City	0.091	6	0.34	0.73	18.19	0.018	FALSE	NST (↑)
Abeokuta	0.182	12	0.75	0.45	18.47	0.036	FALSE	NST (↑)
Akure	0.091	6	0.34	0.73	19.06	0.014	FALSE	NST (↑)
Ibadan	0.061	4	0.21	0.84	18.79	0.018	FALSE	NST (↑)
Asaba	-0.121	-8	-0.48	0.63	19.04	-0.016	FALSE	NST (↓)
Calabar	0.091	6	0.34	0.19	18.19	0.018	FALSE	NST (↑)
Ikeja	-0.091	-6	-0.34	0.73	17.92	-0.029	FALSE	NST (↓)
Uyo	-0.152	-10	-0.62	0.54	17.18	-0.009	FALSE	NST (↓)
Yenagoa	-0.333	-22	-1.77	0.15	17.33	-0.050	FALSE	NST (↓)

*Note: Significance level = 5% (0.05); (↑) indicates an increasing variation and (↓) indicates a decreasing variation; NST - no significant trend

Table 3. The M-K trend test results for average ambient temperature showing the nature of each of their across all years (2005 - 2016).

Location	Kendall's Tau	Mann Kendall's Statistic (S)	Test Statistic (S)	p-value (Two-tailed)	Intercept	Sen's slope (Q)	Test Interpretation	trend
Abakiliki	-0.20	-13	-0.82	0.41	26.45	-0.049	FALSE	NST (↓)
Awka	-0.24	-16	-1.03	0.30	25.36	-0.038	FALSE	NST (↓)
Enugu	-0.21	-14	-0.89	0.37	25.57	-0.052	FALSE	NST (↓)
AdoEkiti	0.02	1	0.00	1.00	24.16	$2.22\times^{-16}$	FALSE	NST (↑)
Umuahia	-0.33	-22	-1.44	0.15	24.70	-0.036	FALSE	NST (↓)
Abeokuta	0.08	5	0.27	0.78	25.40	0.007	FALSE	NST (↑)
Port Harcourt	-0.18	-12	-0.75	0.45	25.12	-0.018	FALSE	NST (↓)
Owerri	-0.18	-12	-0.75	0.45	24.82	-0.020	FALSE	NST (↓)
Akure	-0.08	-5	-0.27	0.78	24.91	-0.005	FALSE	NST (↓)
Ibadan	0.00	0	0.00	1.00	25.38	0.001	FALSE	NST (↑)
Benin City	-0.30	-20	-1.30	0.19	25.17	-0.020	FALSE	NST (↓)
Osogbo	0.03	2	0.07	0.95	24.09	0.004	FALSE	NST (↑)
Asaba	-0.27	-18	-1.17	0.24	25.86	-0.025	FALSE	NST (↓)
Calabar	-0.29	-19	-1.24	0.22	25.59	-0.023	FALSE	NST (↓)
Ikeja	-0.29	-19	-1.24	0.22	26.79	-0.017	FALSE	NST (↓)
Uyo	-0.24	-16	-1.03	0.30	25.08	-0.025	FALSE	NST (↓)
Yenagoa	-0.21	-14	-0.89	0.37	25.46	-0.023	FALSE	NST (↓)

*Note: Significance level = 5% (0.05); (↑) indicates an increasing variation and (↓) indicates a decreasing variation; NST - no significant trend

relatively similar, with highest values for both the radiation and temperature observed in its most recent year (2016).

The hottest locations in the mangrove swamp region for the annual trends from Figure 5e are Ikeja and Asaba, and this corresponds to the locations with the highest radiation in Figure 5b. The same could be said for Abakiliki in Figures 5a and 5d for

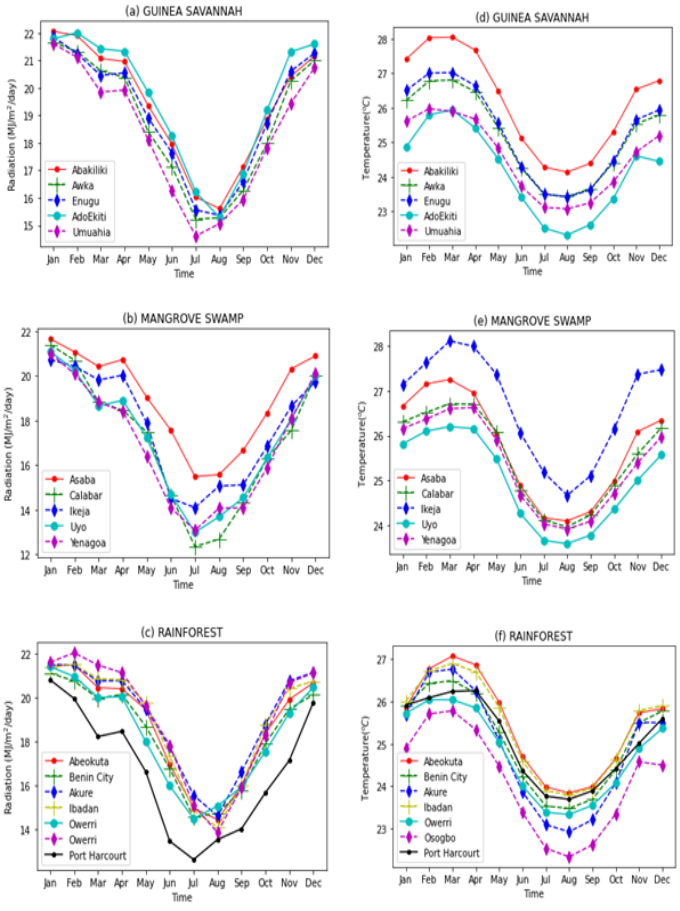

Figure 2. Monthly trend of radiation for all eco-climatic locations (a) Guinea Savannah (b) Mangrove swamp and (c) Rainforest; average ambient temperature trends (d) Guinea Savannah (e) Mangrove swamp and (f) Rainforest.

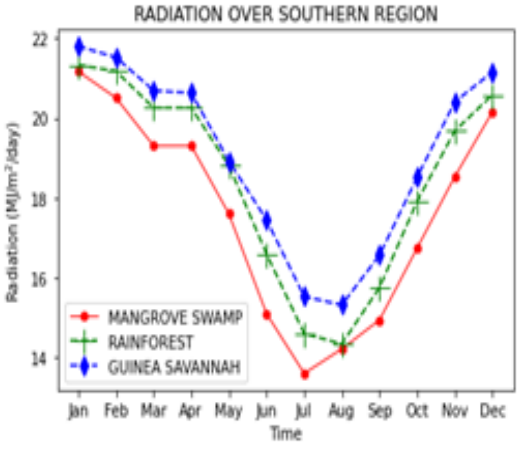

Figure 3. Monthly trend of radiation for all eco-climatic zones in southern Nigeria.

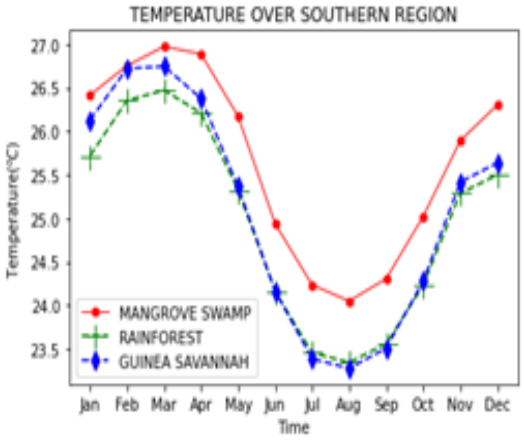

Figure 4. Monthly trend of temperature for all eco-climatic zones in southern Nigeria.

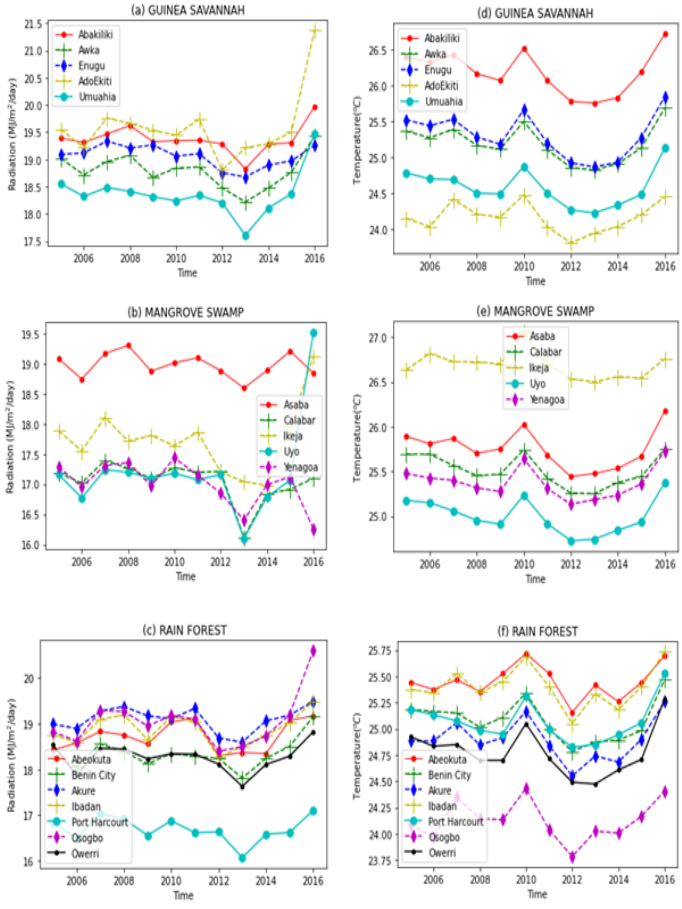

Figure 5. Annual trend of radiation for all eco-climatic locations (a) Guinea Savannah (b) Mangrove swamp and (c) Rainforest; average ambient temperature trends (d) Guinea Savannah (e) Mangrove swamp and (f) Rainforest.

the guinea savannah zone, where the location of highest temperature corresponds to that of highest global solar radiation. The elevation height of the locations is a contributing factor to the temperature values as observed from the figures. It extension, Ikeja shows that a low radiation value is contributed by a location's proximity to a water body, directly related to the sea level.

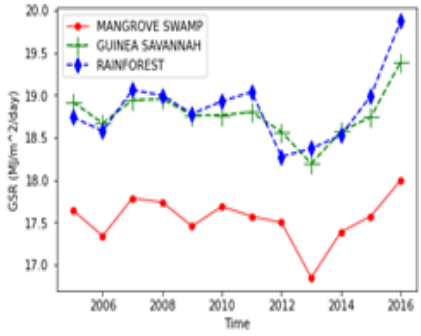

Figure 6. Annual trends of radiation for all southern regions.

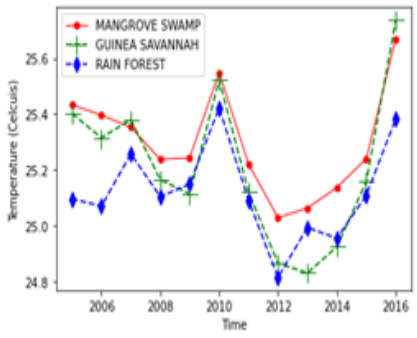

Figure 7. Annual trends of average ambient temperature for all southern regions.

Mann-Kendall trend test

The M-K test has been adopted to analyze the significance of the trends of radiation and average ambient temperature along with Sen's slope (Q). Results presented in Table 2 shows that the results for all locations in each vegetation zone for global solar radiation and in Table 3 for ambient temperature. Significance level of 5% (0.05) was used for the test.

For the global solar radiation trends from Table 2, we can see that all locations in the Mangrove swamp vegetation region all have reducing trends apart from Calabar, characterized by their negative Sen's slope. Apart from Calabar, they all have negative Sen's slope value.

The same reducing radiation trends can be observed in Owerri and Port Harcourt for the Rain Forest vegetation zone after showing negative Z values also. Five of the six locations that have increasing trends are in the Rain Forest vegetation region, these locations are characterized by their positive Sen's slope and Kendall Z values. They include Abeokuta, Akure, Ibadan, Osogbo and Benin City for the SW region having Z values of 0.75, 0.34, 0.21, 0.21 and 0.34 respectively. This shows that the Rain forest vegetation region is majorly characterized by increased radiation trends.

For the ambient temperature trends from table 3, as was similar with that of the radiation results, all locations in the Mangrove swamp vegetation region have reducing trends, characterized by their negative Sen's slope. They have a Z-statistic value of -1.17, -1.24, -1.24, -1.03, -0.89 for Asaba, Calabar, Ikeja, Uyo, Yenagoa respectively.

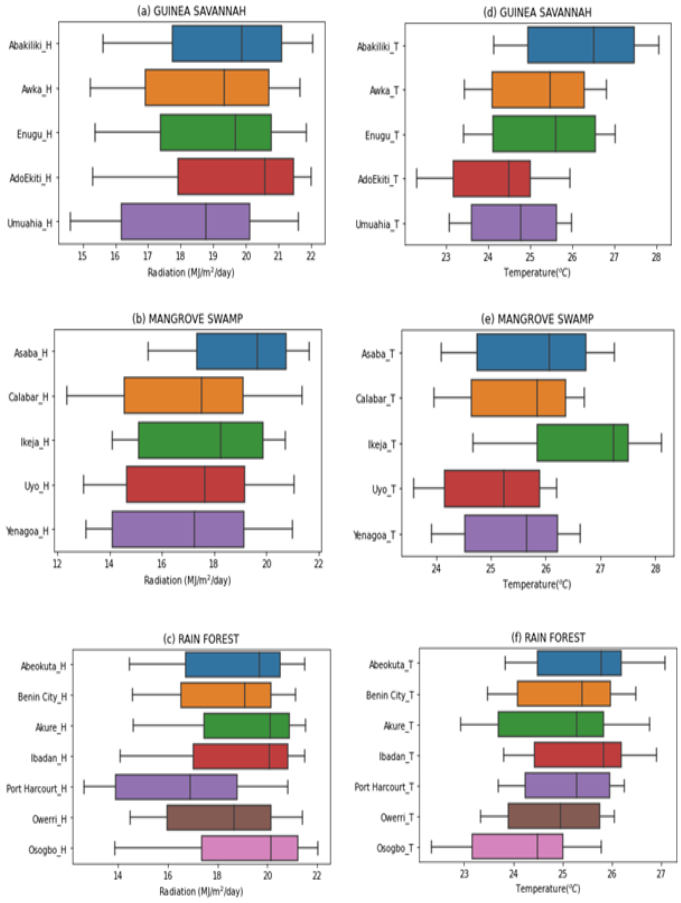

Figure 8. Box plots showing radiation distribution for all eco-climatic locations (a) Guinea Savannah (b) Mangrove swamp and (c) Rainforest; average ambient temperature distributions (d) Guinea Savannah (e) Mangrove swamp and (f) Rainforest.

In the same way as the Mangrove vegetation region, the Guinea Savannah vegetation region also shows reducing temperature trends. This shows the similarity between the Mangrove vegetation region and the Guinea Savannah region.

The Rain forest vegetation region has three (3) locations has increasing trends for ambient temperature, these locations are characterized by their positive Sen's slope and Kendall Z values. They include Abeokuta, Ibadan and Osogbo of the Rain forest vegetation zone having Z values of 0.27, 0, and 0.07. The results for majority of these locations for temperature in table 3 approximately corresponds relatively to that of global solar radiation in Table 2.

At 5% significance level, all radiation and temperature variations accepted the null hypothesis H_o and rejected the alternative hypothesis H_1 after its probability value (p-value) of these series (increasing or decreasing) was found to be more than the significance level $\alpha = 0.05$. This means that although most figures reducing or increasing variations, this increase or decrease aren't occurring with much significance.

4.3. Box Plots

To discern the distribution of radiation and temperature for all locations, box plots have presented in Figures 8 (a – f) and 9

Table 4. Linear regression results for all Mangrove swamp locations.

	Asaba	Calabar	Ikeja	Uyo	Yenagoa
Correlation (R)	0.95	0.92	0.89	0.92	0.88
Slope	1.75	2.65	1.87	2.46	2.36
Error in slope	0.19	0.36	0.30	0.34	0.40
R^2	0.89	0.84	0.80	0.84	0.78
Intercept (C)	-26.07	-50.53	-32.05	-44.30	-42.77
Error in C	4.89	9.32	7.90	8.51	10.13
SD	0.75	1.27	1.18	1.15	1.37

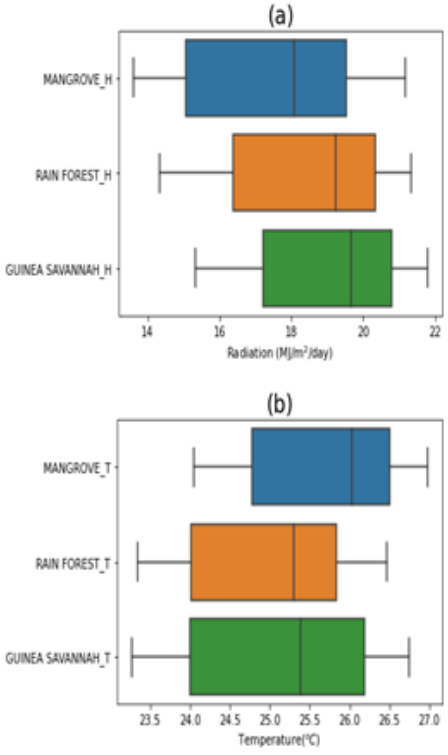

Figure 9. Box plots showing the average (a) radiation and (b) temperature distribution over each southern eco-climatic zone.

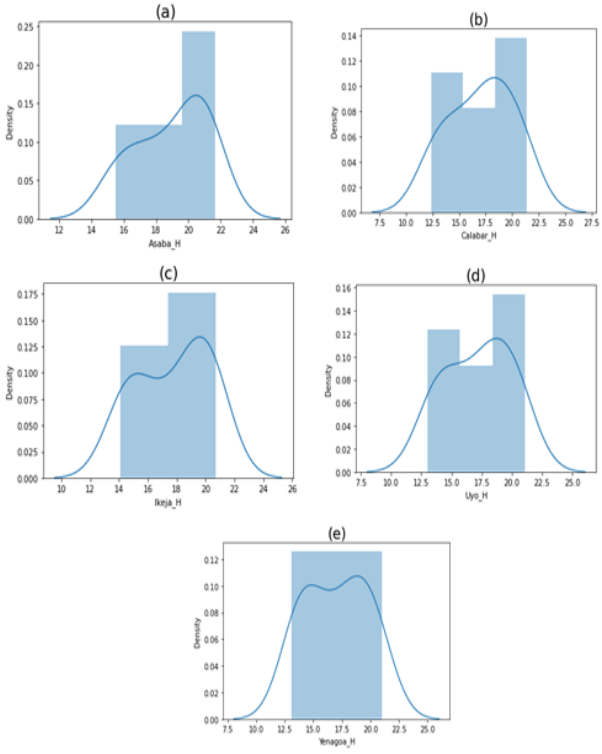

Figure 10. KDE plots showing radiation distribution in $MJ/m^2/day$ for all locations in the Mangrove swamp zone (a) Asaba (b) Calabar (c) Ikeja (d) Uyo (e) Yenagoa.

Table 5. Linear regression results for all Guinea savannah locations.

	Abakiliki	Awka	Enugu	Ado-Ekiti	Umuahia
Correlation (R)	0.95	0.95	0.93	0.93	0.94
Slope	1.45	1.76	1.55	1.74	2.04
Error in slope	0.15	0.18	0.19	0.22	0.23
R^2	0.91	0.90	0.86	0.86	0.89
Intercept (C)	-18.59	-25.49	-20.08	-22.47	-31.82
Error in C	3.85	4.65	4.91	5.28	5.67
SD	0.72	0.79	0.89	0.93	0.86

Table 6. Linear regression results for all SW locations.

	Abeokuta	Benin City	Akure	Ibadan	Owerri	Osogbo	Port Harcourt
Correlation (R)	0.91	0.96	0.93	0.94	0.95	0.95	0.90
Slope	1.94	1.96	1.61	2.13	2.18	2.17	2.55
Error in slope	0.29	0.18	0.20	0.25	0.23	0.21	0.38
R^2	0.82	0.92	0.87	0.87	0.90	0.91	0.82
Intercept (C)	-30.67	-30.71	-21.02	-35.19	-35.82	-33.22	-47.34
Error in C	7.33	4.57	4.94	6.47	5.62	5.15	9.63
SD	1.12	0.69	0.92	0.98	0.79	0.88	1.27

(a and b). A careful observation of the box plots show that their distribution for some locations is almost similar, characterized by a median that is almost uniform.

Figures 8a and 8d shows the radiation and temperature distribution respectively for all locations in the guinea savannah zone. Similar to that of locations in the mangrove swamp zone, all boxes representing radiation in the Guinea savannah zone (from Figure 8a), shows that the peak radiation value for all locations is approximately equal. However, for the temperature distribution in Figure 8d, Abakiliki has the highest temperature value for all locations in the SE, with Umuahia and Ado-Ekiti having the lowest.

The representation for the radiation and temperature in Figures 8b and 8e respectively for the Mangrove swamp zone shows that Asaba has the highest radiation and temperature value; this corresponds to results of our monthly and annual line plots. The

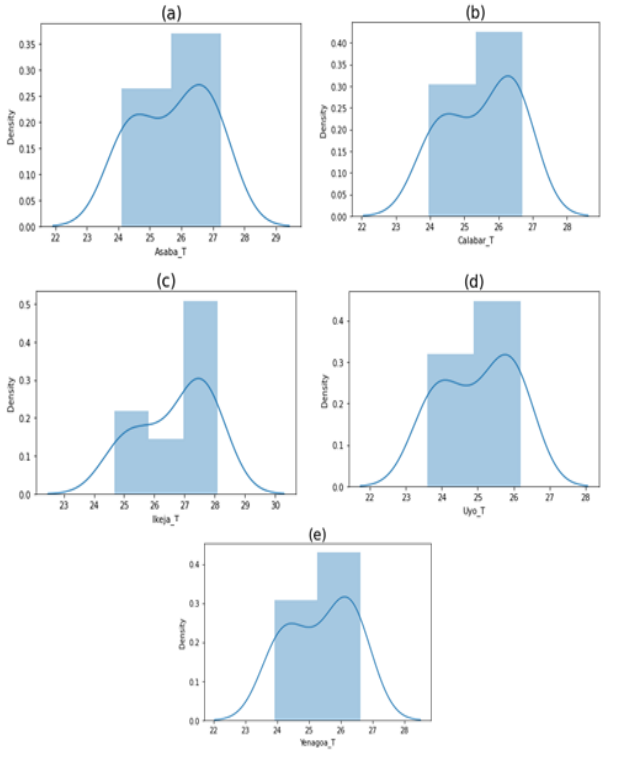

Figure 11. KDE plots showing temperature distribution in Celsius for all locations in the Mangrove swamp zone (a) Asaba (b) Calabar (c) Ikeja (d) Uyo (e) Yenagoa.

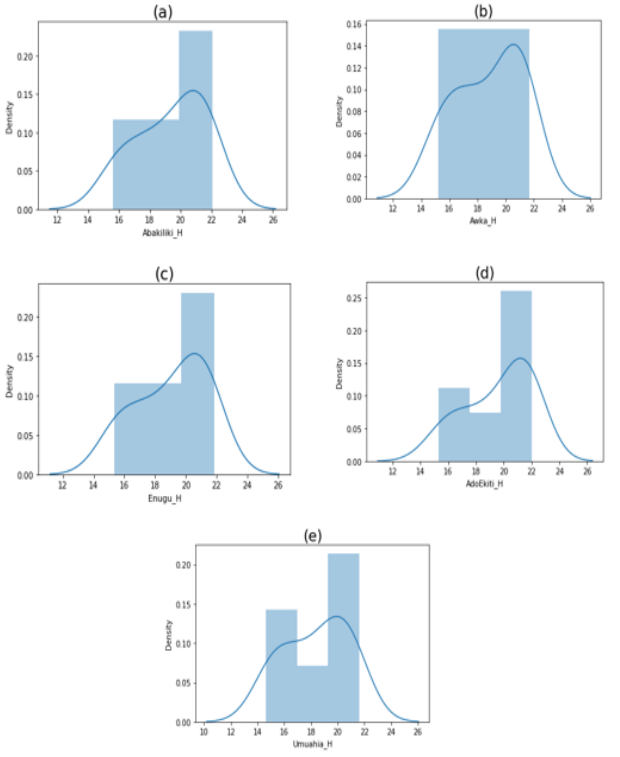

Figure 12. KDE plots showing radiation distribution in $MJ/m^2/day$ for all locations in the Guinea savannah zone (a) Abakiliki (b) Awka (c) Enugu (d) Ado-Ekiti (e) Umuahia.

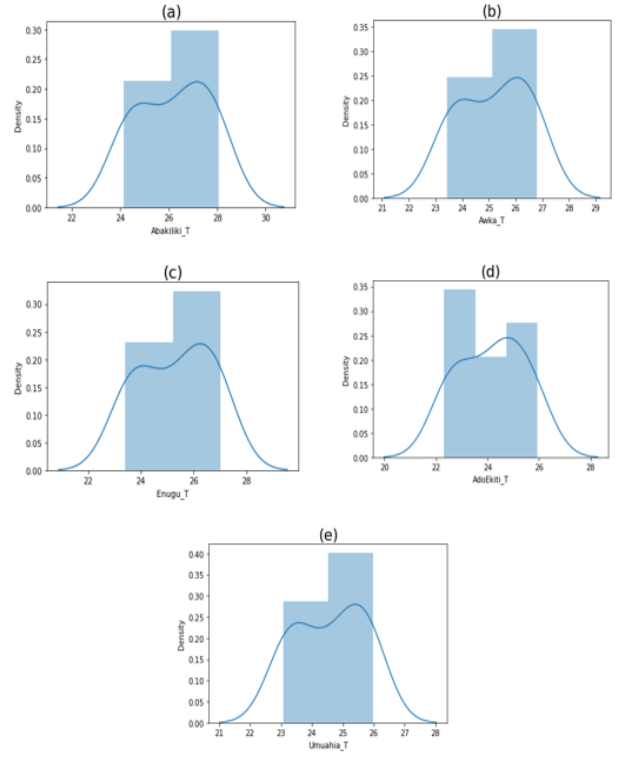

Figure 13. KDE plots showing temperature distribution in Celsius for all locations in the Guinea savannah zone (a) Abakiliki (b) Awka (c) Enugu (d) Ado-Ekiti (e) Umuahia.

temperature representations in the Figure 8e for each location has relatively smaller ranges than that of the radiation plot in Figure 8e. This could be attributed to the fact that it takes a certain threshold of temperature to bring about a notable shift in radiation [36]. All location in the mangrove swamp zone all have approximately the same peak radiation values from Figure 8b, but the same cannot be said for the temperature plot in Figure 8e.

Figures 8c and 8f represents the distribution of radiation and temperature for all locations in the rain forest zone. This region seems to have the widest range of radiation distribution for all her locations from figure 8e. The data distribution range for the temperature however, has some variations. As it was earlier explained in the monthly and annual line plots, Abeokuta in Ogun state has the highest temperature for all locations this region. The range of this box represented in Figure 8f is not also large; hence, the temperature is constantly high. Although scattered across different peak values, all locations in this zone have about the same distribution range from the highest to the lowest value.

All plots in Figure 8 shows that the peak radiation is closely similar which is in contrast with that of the ambient temperature. This observation shows that changes in the peak value of temperature to only results in a radiation peak value that cannot rise above a particular threshold value. This crystalizes the argument that the radiation value of a location is affected by the geographical location (latitude, elevation height) also.

Figure 9 shows the collation of radiation and temperature

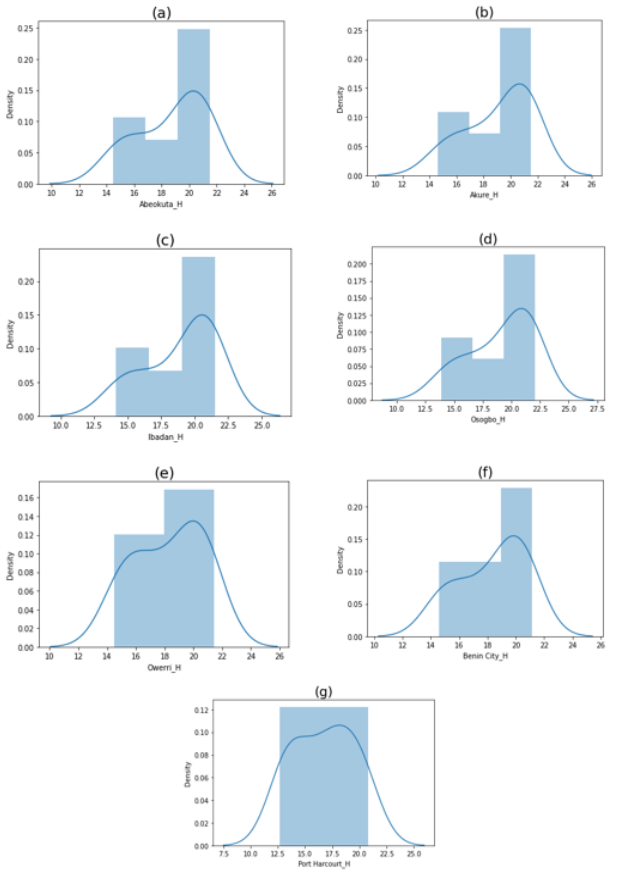

Figure 14. KDE plots showing radiation distribution in $MJ/m^2/day$ for all locations in the Rain Forest zone (a)Abeokuta (b)Awka (c) Ibadan (d) Osogbo (e) Owerri (f) Benin City (g)Port Harcourt.

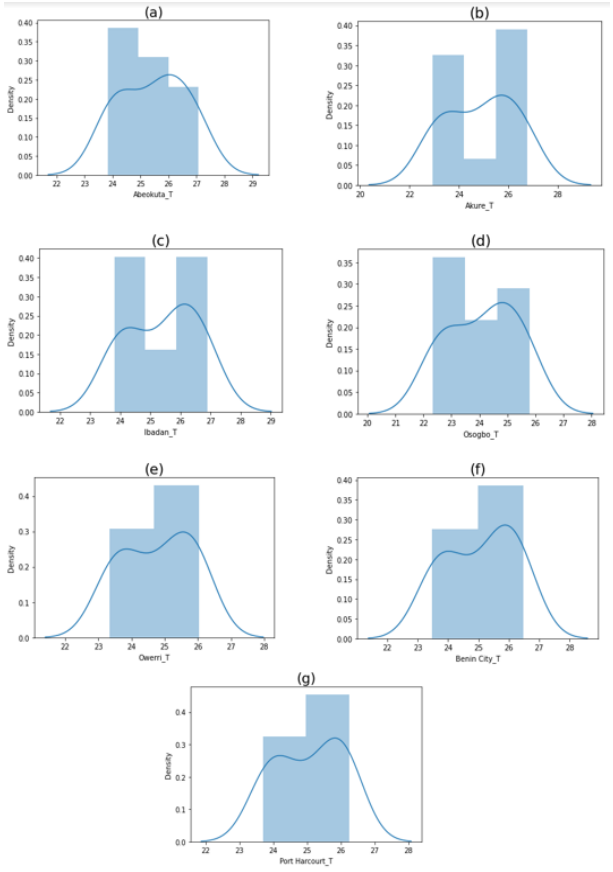

Figure 15. KDE plots showing temperature distribution in Celcuis for all locations in the Rain Forest zone (a)Abeokuta (b)Awka (c) Ibadan (d) Osogbo (e) Owerri (f) Benin City (g)Port Harcourt.

box plots respectively for all zones in the south. The average values of temperature and radiation are well represented in the figure.

The global solar radiation representation from Figure 9a shows that the southern locations have between 14 and 20 $MJ/m^2/day$. Due to the fact that the global solar radiation variation depends majorly on the variation of ambient temperature, we observe higher values of global solar radiation for the guineas savannah and rainforest regions. This is not so for the mangrove swamp zone.

All southern regions had their values within the range of 23 ^oC to 26.5 ^oC from the temperature box plot in Figure 9b. Relating to the radiation plot in Figure 9, the mangrove swamp region's close proximity to the Atlantic Ocean bring about the low temperature ranges, even though judging from the latitude of the region (closest to the equator), it should be slightly hotter.

4.4. Univariate KDE

Distribution plots for temperature and global solar radiation for all locations being studied has been well represented (Figures 10 - 16). The univariate Gaussian (normal) distribution was carried out to show the density of data distribution as well as to show the modal peaks and skewness of the distribution. The purpose of these plots is to show how the temperature and radiation data is being distributed across the data range, revealing the median, modal peak(s)/densities, etc.

Figures 10 show the radiation distribution for locations in the mangrove swamp zone. All locations seem to have at least a modal peak at about 20 $MJ/m^2/day$. Yenagoa have 2 modal peaks while Calabar and Uyo have the same distribution and density from the figure. The similarity between these pair of regions arises from the fact that they are in close proximity to each other.

The temperature distributions for all locations in the mangrove swamp zone (Figure 11) all have the same Gaussian distribution. Their densities peak at approximately 0.27 and they all have 2 modal peaks. The uniformity in the distributions of all temperature representations for the SS zone shows the uniform climatic conditions in the region.

From Figure 12, we see the radiation distributions for all locations in the guinea savannah locations. Similar to the mangrove swamp locations, the modal peak lies round 20 $MJ/m^2/day$, showing the similarity between the locations. In particular, the density/Gaussian distributions for Abakiliki, Enugu and Umuahia are more similar with each other, having a peak density value of about 0.15 around their modal peak.

The temperature distribution locations in the guinea savannah zone (Figure 13) like that of the mangrove swamp zone. is

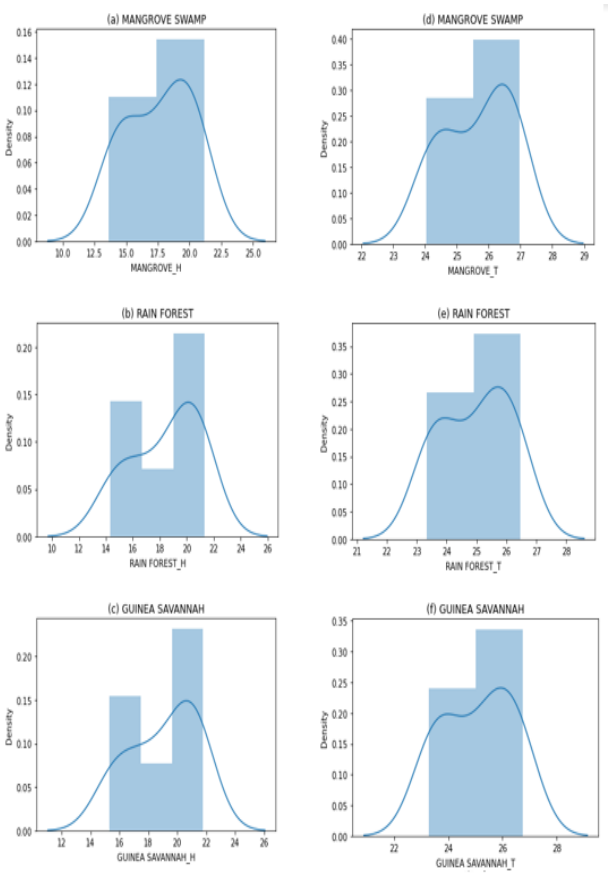

Figure 16. KDE plots showing distributions for all eco-climatic regions in the south for global solar radiation (a) Mangrove swamp (b) Rain Forest (c) Guniea savannah; and temperature (d) Mangrove swamp (e) Rain Forest (f) Guniea savannah.

similar across all locations in the same zone. The distribution is the same with a Gaussian distribution that has 2 close modal peaks; this shows the data spread across range of values. The homogeneity in the distributions of all temperature representations for the guinea savannah zone shows the uniform climatic conditions in the region just as was in that of the mangrove swamp.

Figure 14 shows the radiation distribution for all locations in the rain forest region. Contrary to other zones (mangrove swamp and guinea savannah), the locations in the rain forest have a more similar density (Gaussian) distribution.

The temperature distribution for all locations in the rainforest zone (Figure 15) is not a similar as of that for all locations in the mangrove swamp and guinea savannah zones. All locations show relatively similar Gaussian distributions.

Figure 16 shows the combined distribution plots for temperature and radiation for all the southern zones. The density (KDE) plots for the global solar radiation for the Mangrove swamp, Rain Forest, and Guniea savannah (Figures 16a, 16b and 16c respectively) follows similar curves with that of the ambient temperature (Figures 16d, 16e and 16f respectively). This shows a strong positive coefficient of correlation between the global solar radiation and temperature for each zone.

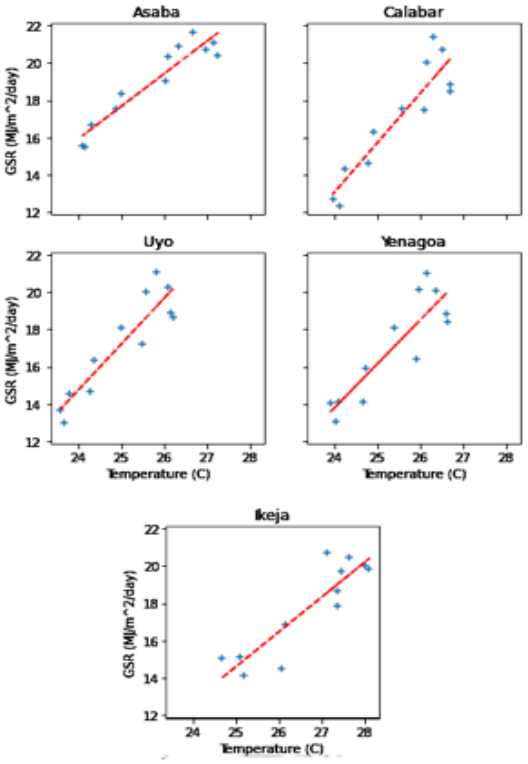

Figure 17. Regression plots showing the relationship between radiation and temperature for all locations in the Mangrove swamp zone.

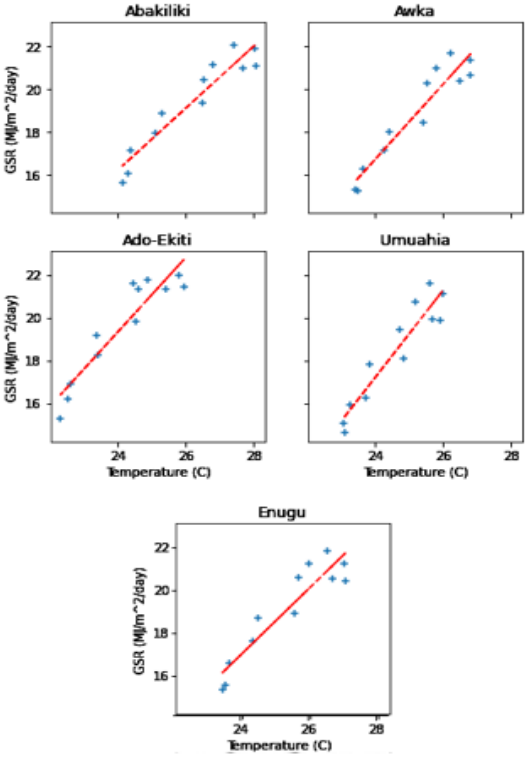

Figure 18. Regression plots showing the relationship between radiation and temperature for all locations in the Guinea savannah zone.

4.5. *Linear Regression*

The goal of the linear regression to understand the relationship between the variation of ambient temperature and global

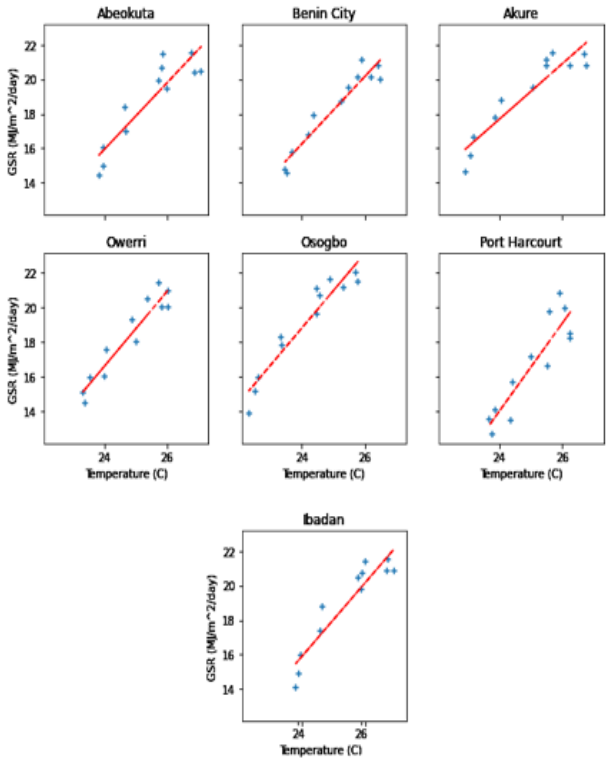

Figure 19. Regression plots showing the relationship between radiation and temperature for all locations in the Rain Forest zone.

solar radiation for all locations in each zone. The same scale was used for the plots to show the discrepancies in the trend lines. The independent variable was the temperature and the radiation was the dependent variable. Results from the regression analysis have also be well represented in tables including the coefficient of correlation (R), Coefficient of determination (R^2), slope, error in slope, intercept, error in intercept. standard deviation.

From Figure 17, we can see the regression plots for all locations in the mangrove swamp zone. Table 4 shows the results from the regression. Asaba has the strongest relationship between radiation and temperature; characterized by its strong positive R value (the strongest for the zone), lowest error in slope and standard deviation from the mean. Other locations in the mangrove swamp zone from the figure all have strong positive values of R also. Since we used the same scale to plot for all locations in the region, we can see the differences in the radiation and temperature spread across the y and x axes respectively. This spread agrees with results from the box plots for the zone (Figures 8b and 8e). Yenagoa, although having a strong positive R value (0.88), represents the lowest in the mangrove swamp zone.

Figure 18 represents the regression plots for all locations in the guinea savannah region. Table 5 shows the results from this regression. We can observe from the trend that all locations have an almost similar relationship between radiation and temperature. This is characterized by the similar R value for all 5 locations in the region (R values ranges between 0.93 and 0.95). This very strong positive R value corresponds to lower errors in the slope and intercept of the trends, as well as the standard deviation (Table 5). This means that the guinea savannah zone constitutes the strongest relationship between global solar radiation and temperature for all zones.

Figure 19 represents the regression plots for all locations in the SW region. Table 6 shows the results from this regression. From our results, Benin City has the strongest positive R value (0.96), followed by Owerri and Osogbo Ibadan (0.95 each). The lowest R value is observed in Port Harcourt (0.90). This is so because from our box plot results for radiation and temperature in figure 8c and 8f respectively, a high temperature value for Port Harcourt does not bring about a high radiation value for the same location in the region.

In conclusion, all southern locations have strong positive relationships between radiation and temperature. This proves that for any change in the temperature variations in the region, there is a corresponding strong similar change in the global solar radiation variation [37, 38].

5. Conclusion

We have shown the relationship between the variation of solar irradiation and average ambient temperature for locations in the eco-climatic zones in the south of Nigeria. This region is made up of 17 locations and 2 eco-climatic zones (mangrove swamp, guinea savannah and tropical rainforest). The study was done to have a better understanding of the trends, distributions and relationships between the two variables. The Mann-Kendall trend test has been used to study the significance of the variations of both variables in all regions and in general the following results and inferences were outlined.

- The trends of solar irradiance and ambient temperature for all stations and eco-climatic zones are not increasing or decreasing annually with significance from the results of the MK test.
- Linear regression, and distribution plots depict the positive relationship between both variables (Global solar radiation and temperature) across all stations, albeit, some variations in the strong positive correlation for some locations were observed. This may be attributed to the differences in elevation height, climatic conditions, and local weather, etc.
- Results show that the climate and vegetation of a region contributes majorly to the variation of radiation and temperature. Inhomogeneity of data or results for locations in the same zones may be attributed to local meteorological conditions and effects like carbon emission from industries, proximity to major water bodies, etc.
- Although 12 years' data might not be sufficient to conclude in terms of climatological conditions, the results show that meteorological conditions of the study locations are almost uniform in variation. This proves that latitudinal locations are one of the major contributors to

global solar radiation and temperature variations, especially for locations that are relatively close in geographical proximity.

Acknowledgments

We thank the referees for the positive enlightening comments and suggestions, which have greatly helped us in making improvements to this paper.

Code Availability: The code associated with this analysis can be assessed from https://github.com/Emmaestro001/JNSPS-Article-Analysis.

Data Availability: The data associated (temperature and global solar radiation) with this study was obtained from the PVGIS (photovoltaic geographical information system) for twelve years (2005-2016) at https://re.jrc.ec.europa.eu/pvg_tools/en?tools.html#PVP.

References

[1] M. Irfan, R. M. Elavarasan, Y. Hao, M. Feng, & D. Sailan, "An assessment of consumers' willingness to utilize solar energy in China: End-users' perspective", Journal of Cleaner Production, **292** (2021) 126008. https://doi.org/10.1016/j.jclepro.2021.126008.

[2] H. Eroğlu, "Development of a novel solar energy need index for identifying priority investment regions: a case study and current status in Turkey", Environment, Development and Sustainability, (2021) 1. https://doi.org/10.1007/s10668-021-01812-3.

[3] A. A. Adenle, "Assessment of solar energy technologies in Africa-opportunities and challenges in meeting the 2030 agenda and sustainable development goals", Energy Policy, **137** (2020) 111180. https://doi.org/10.1016/j.enpol.2019.111180.

[4] E. P. Agbo, C. O. Edet, T. O Magu, A. O. Njok, C. M. Ekpo & H. Louis, "Solar energy: A panacea for the electricity generation crisis in Nigeria", Heliyon, **7** (2021) e07016.https://doi.org/10.1016/j.heliyon.2021.e07016.

[5] J. Lee, & M. M. Shepley, "Benefits of solar photovoltaic systems for low-income families in social housing of Korea: Renewable energy applications as solutions to energy poverty", Journal of Building Engineering, **28** (2020) 101016. https://doi.org/10.1016/j.jobe.2019.101016.

[6] P. K. Adom, F. Amuakwa-Mensah, M. P. Agradi, & A. Nsabimana, "Energy poverty, development outcomes, and transition to green energy", Renewable Energy, **178** (2021) 1337. https://doi.org/10.1016/j.renene.2021.06.120.

[7] H. Tao, A. A. Ewees, A. O. Al-Sulttani, U. Beyaztas, M. M. Hameed, S. Q. Salih, & Z. M. Yaseen, "Global solar radiation prediction over North Dakota using air temperature: development of novel hybrid intelligence model", Energy Reports, **7** (2021) 136. https://doi.org/10.1016/j.egyr.2020.11.033.

[8] L. Yu, M. Zhang, L. Wang, Y. Lu, & J. Li, "Effects of aerosols and water vapour on spatial-temporal variations of the clear-sky surface solar radiation in China" Atmospheric Research, **248** (2021) 105162. https://doi.org/10.1016/j.atmosres.2020.105162.

[9] O. Rejeb, M. S. Yousef, C. Ghenai, H. Hassan, & M. Bettayeb, "Investigation of a solar still behaviour using response surface methodology", Case Studies in Thermal Engineering, **24** (2021) 100816. https://doi.org/10.1016/j.csite.2020.100816.

[10] M. A. Yamasoe, N. M. E. Rosário, S. N. S. M. Almeida, & M. Wild, "Fifty-six years of surface solar radiation and sunshine duration over São Paulo, Brazil: 1961–2016" Atmospheric Chemistry and Physics, **21** (2021) 6593. https://doi.org/10.5194/acp-21-6593-2021.

[11] Ü. Ağbulut, A. E. Gürel, & Y. Biçen, "Prediction of daily global solar radiation using different machine learning algorithms: Evaluation and comparison", Renewable and Sustainable Energy Reviews, **135** (2021) 110114. https://doi.org/10.1016/j.rser.2020.110114.

[12] A. E. Lawin, M. Niyongendako, & C. Manirakiza, "Solar irradiance and temperature variability and projected trends analysis in Burundi", Climate, **7** (2019) 83. https://doi.org/10.3390/cli7060083.

[13] J. L. Lean. "Cycles and trends in solar irradiance and climate. Wiley interdisciplinary reviews: climate change" **1** (2010) 111. https://doi.org/10.1002/wcc.18.

[14] L. Qian, C. Jacobi, J. McInerney, "Trends and solar irradiance effects in the mesosphere", Journal of Geophysical Research: Space Physics, **124** (2019) 1343. https://doi.org/10.1029/2018JA026367.

[15] B. Mendoza, "Total solar irradiance and climate", Advances in Space Research, **35** (2005) 882. https://doi.org/10.1016/j.asr.2004.10.011.

[16] W. Soon, D. R. Legates, "Solar irradiance modulation of Equator-to-Pole (Arctic) temperature gradients: Empirical evidence for climate variation on multi-decadal timescales", Journal of Atmospheric and Solar-Terrestrial Physics, **93** (2013) 45. https://doi.org/10.1016/j.jastp.2012.11.015.

[17] A. J. Aparicio, M. C. Gallego, M. Anton, J. M. Vaquero, "Relationship between solar activity and direct solar irradiance in Madrid (1910–1929)", Atmospheric Research, **235** (2020) 104766. https://doi.org/10.1016/j.atmosres.2019.104766.

[18] A. Bhargawa, A. K. Singh, "Solar irradiance, climatic indicators and climate change–An empirical analysis" Advances in Space Research, **64** (2019) 271. https://doi.org/10.1016/j.asr.2019.03.018.

[19] H. T. Abdulkarim, C. L. Sansom, K. Patchigolla, & P. King, "Statistical and economic analysis of solar radiation and climatic data for the development of solar PV system in Nigeria", Energy Reports **6** (2020) 309. https://doi.org/10.1016/j.egyr.2019.08.061.

[20] V. N. Dike, T. C. Chineke, O. K. Nwofor, and U. K. Okoro, "Evaluation of horizontal surface solar radiation levels in southern Nigeria", Journal of renewable and sustainable energy, **2** (2011) 023101. https://doi.org/10.1063/1.3558871.

[21] O. S. Ohunakin, M. S. Adaramola, O. M. Oyewola, & R. O. Fagbenle, "Correlations for estimating solar radiation using sunshine hours and temperature measurement in Osogbo, Osun State, Nigeria", Frontiers in Energy, **7** (2013) 214. https://doi.org/10.1007/s11708-013-0241-2.

[22] M. S. Okundamiya, J. O. Emagbetere, & E. A. Ogujor. "Evaluation of various global solar radiation models for Nigeria", International Journal of Green Energy, **13** (2016) 505. https://doi.org/10.1080/15435075.2014.968921.

[23] C. B. Do, "The multivariate Gaussian distribution. Section Notes" Lecture on Machine Learning, CS, **229** (2008).

[24] M. N. Lang, G. J. Mayr, R. Stauffer, & A. Zeileis, "Bivariate Gaussian models for wind vectors in a distributional regression framework", Advances in Statistical Climatology, Meteorology and Oceanography **5** (2019) 115. https://doi.org/10.5194/ascmo-5-115-2019.

[25] E. P. Agbo, "The role of statistical methods and tools for weather forecasting and modeling" [Online First]. In Weather Forecassting. IntechOpen, https://doi.org/10.5772/intechopen.96854.

[26] A. Mondal, S. Kundu, & A. Mukhopadhyay "Rainfall trend analysis by Mann-Kendall test: A case study of north-eastern part of Cuttack district, Orissa", International Journal of Geology, Earth and Environmental Sciences **2** (2012) 70.

[27] E. P. Agbo, C. M. Ekpo, "Trend Analysis of the Variations of Ambient Temperature Using Mann-Kendall Test and Sen's Estimate in Calabar, Southern Nigeria" (2020) Researchgate Preprint. https://doi.org/10.13140/RG.2.2.26163.04644.

[28] E. P. Agbo, C. M. Ekpo, "Trend Analysis of the Variations of Ambient Temperature Using Mann-Kendall Test and Sen's Estimate in Calabar, Southern Nigeria" In Journal of Physics: Conference Series. IOP Publishing, **1734** (2021) p012016. https://doi.org/10.1088/1742-6596/1734/1/012016.

[29] U. U. Alhaji, A. S. Yusuf, C. O. Edet, C. O. Oche, E. P. Agbo, "Trend analysis of temperature in Gombe state using Mann Kendall Trend test", Journal of Scientific Research and Reports **20** (2018) 1. https://doi.org/10.9734/JSRR/2018/42029.

[30] N. Khanmohammadi, H. Rezaie, & J. Behmanesh, "The effect of autocorrelation on the meteorological parameters trend" Meteorology and Atmospheric Physics **133** (2021) 565. https://doi.org/10.1007/s00703-020-00762-1.

[31] E. P Agbo, C. M. Ekpo, C. O. Edet, "Analysis of the effects of meteorological parameters on radio refractivity, equivalent potential temperature and field strength via Mann-Kendall test", Theor Appl Climatol., (2021). https://doi.org/10.1007/s00704-020-03464-1.

[32] E. P. Agbo, E. B. Ettah, E. E. Eno, "The impacts of meteorological param-

eters on the seasonal, monthly and annual variation of radio refractivity" Indian J Phys (2020) https://doi.org/10.1007/s12648-020-01711-9.

[33] O. O. Soneye, M. A. Ayoola, I. A. Ajao, & O. O. Jegede. "Diurnal and seasonal variations of the incoming solar radiation flux at a tropical station, Ile-Ife, Nigeria", Heliyon, **5** (2019) e01673. https://doi.org/10.1016/j.heliyon.2019.e01673.

[34] O. S. Ohunakin, M. S. Adaramola, O. M. Oyewola, O. J. Matthew, & R. O. Fagbenle. "The effect of climate change on solar radiation in Nigeria", Solar Energy, **116** (2015) 272. https://doi.org/10.1016/j.solener.2015.03.027.

[35] O. M. Akinbode, A. O. Eludoyin, O. A. Fashae. "Temperature and relative humidity distributions in a medium-size administrative town in southwest Nigeria", Journal of environmental management, **87** (2008) 95. https://doi.org/10.1016/j.jenvman.2007.01.018.

[36] R. Knutti, & G, C. Hegerl. "The equilibrium sensitivity of the Earth's temperature to radiation changes", Nature Geoscience, **1** (2008) 735. https://doi.org/10.1038/ngeo337.

[37] M. Wild, D. Folini, F. Henschel, N. Fischer, & B. Müller. "Projections of long-term changes in solar radiation based on CMIP5 climate models and their influence on energy yields of photovoltaic systems", Solar Energy, **116** (2015) 12. https://doi.org/10.1016/j.solener.2015.03.039.

[38] D. J. Mildrexler, M. Zhao, and S. W. Running. "A global comparison between station air temperatures and MODIS land surface temperatures reveals the cooling role of forests", Journal of Geophysical Research: Biogeosciences, **116** (2011). https://doi.org/10.1029/2010JG001486.